Method of evaluation of a mirror surface figure based on frequency domain and its application for the Giant Steerable Science Mirror of the Thirty Meter Telescope

Fei Yang (杨 飞)[1,2,*], Guojun Liu (刘国军)[1], Qichang An (安其昌)[2], and Xuejun Zhang (张学军)[2]

[1]*State Key Laboratory of High Power Semiconductor Lasers, Changchun University of Science and Technology, Changchun 130022, China*

[2]*Changchun Institute of Optics, Fine Mechanics and Physics, Chinese Academy of Sciences, Changchun 130033, China*

**Corresponding author: yangf@ciomp.ac.cn*

Received October 14, 2014; accepted January 28, 2015; posted online April 7, 2015

We propose a sub-aperture stitching algorithm based on a frequency domain that can be denoted as a power spectral density (PSD). Our algorithm is verified by the experimental data obtained from measuring a Φ1.23 m mirror at the Changchun Institute of Optics, Fine Mechanics and Physics. Then, we apply it to the Great Steering Science Mirror (GSSM) of the Thirty Meter Telescope (TMT) with the simulated data before the preliminary design phase, and obtain a more objective result on the frequency domain aberrations. Therefore, the sub-aperture stitching-based PSD is expected to be useful for specifying a large aperture mirror surface for mirror vendors.

OCIS codes: 120.3940, 110.6770, 110.3925.
doi: 10.3788/COL201513.041201.

The Thirty Meter Telescope (TMT) project is an international partnership between the California Institute of Technology, the University of California, and the Association of Canadian Universities for Research in Astronomy, which has been joined by the National Astronomical Observatory of Japan, the National Astronomical Observatories of the Chinese Academy of Sciences, and the Department of Science and Technology of India. The Changchun Institute of Optics, Fine Mechanics and Physics is responsible for the research and development of the tertiary mirror system for the TMT. The tertiary mirror system has the new name of the Giant Steerable Science Mirror (GSSM) because of its unique function and size. The GSSM has a surface area of 3.594 m × 2.536 m × 0.1 m, and is the first steerable tertiary mirror with such a large size to our knowledge. The traditional evaluation method will not be suitable for such a large aperture mirror surface[1,2].

Time-domain analysis has been widely applied in various small-diameter mirror analyses. To complete a time-domain analysis, all of the time-domain information is needed. Information relating to the element position is also required, but it is only necessary to obtain this information on one dimension. However, this evaluation method has certain limitations when it comes to analyzing a large aperture reflecting mirror[3–5].

Using power spectral density (PSD) as the mirror surface shape evaluation method in the frequency domain was proposed in the last century by the LLNL, USA. However, the diameter of the main PSD application object was too small, and the specific algorithms also needed improvements. Meanwhile, in recent years, some scholars used the root mean square (RMS) slope to characterize the surface undulations of large aperture optical mirrors. To evaluate the frequency characteristics of a large aperture reflecting mirror surface, the project team decided to use slope RMS and PSD to comprehensively evaluate the mirror surface of the GSSM of the TMT[6–9].

The stitching technique is a low-cost, effective means of testing large aperture mirrors at a high resolution. In this Letter, a non-correlated sub-aperture stitching method based on the frequency domain was proposed, and the quality of its estimates was analyzed.

For the sake of simplicity, we assume that the expectations of all wavefront aberrations are zero. Non-zero expectations can be classified as zero expectations through the method of filtering the direct current component using time-domain translation or frequency domain.

Generally, the value of the system wavefront error was obtained using basal polynomial fitting. The standard sinusoidal polynomial is the common base in harmonic analysis. For the standard sinusoidal polynomial, as shown in

$$\Phi = A\,\sin(2\pi f x), \tag{1}$$

the wavefront $\mathrm{RMS}_\Phi = A/\sqrt{2}$ is constant. It can be seen that the RMS is completely free of frequency domain characteristics, so it cannot fully respond to the inside dynamic characteristics for a total-energy wavefront. To solve this problem, we define slope RMS as

$$\text{slope RMS} = \sqrt{2}\pi f A. \tag{2}$$

Suppose that a certain-order harmonic component is dominant in the system wavefront aberrations. Using Eq. (2), we can get the value of

$$f_0 = \frac{\text{slope RMS}}{\sqrt{2}\pi A},$$

which is used as the cutoff frequency of the system. Slope RMS, system transfer function, and structure function have a strong corresponding relationship, as shown in

$$D(r) = 2\sigma_\phi^2(1 - \exp(-(f_o r)^2)), \tag{3}$$

$$\text{OTF}(f) = \exp\left(-\frac{1}{2}k^2 D(\lambda f)\right). \tag{4}$$

The relationship between the cutoff frequency and the structure function is shown in Fig. 1: as the cutoff frequency increases, the high frequency of the system structure function becomes more stringent, and the demands of the grinding of the mirror increase. However, the low frequency of the system (RMS) remains the same, due to the fact that the RMS does not have dynamic characteristics.

When calculating the system's slope RMS, the exact solution can be obtained by using the original definition of the wavefront for information processing. However, the computational time and space costs are difficult to reasonably control. If wavefront fitting first uses a basal polynomial, then analyzes the compositional operations through the relationship between the slope RMS and the basal polynomial, the calculation process can be greatly simplified. It should be noted that the order of polynomials for fitting would not be infinitely high, so the treatment of residuals will be discussed.

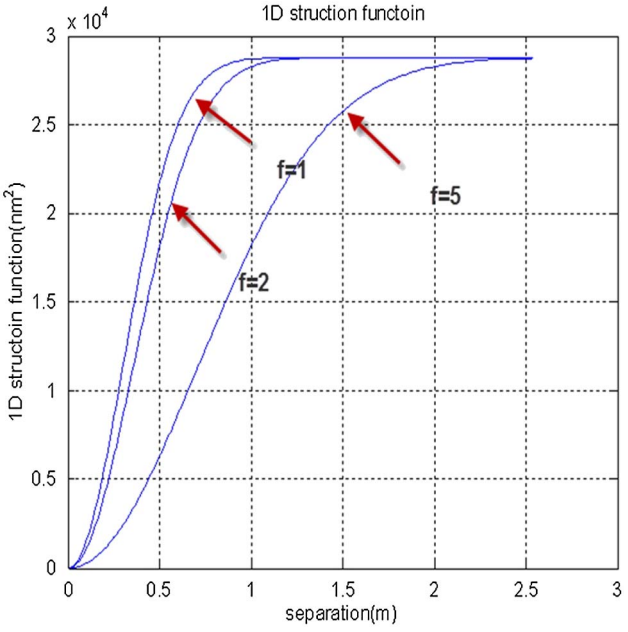

Fig. 1. The relationship between the cutoff frequency and structural function.

First, assume that the system wave aberrations consists of two standard sine polynomials. The slope RMS can be calculated as

$$\Phi = \alpha\sqrt{2}A\,\sin(2\pi f x) + \beta\sqrt{2}A\,\sin(2\pi 2 f x),$$
$$\text{slope RMS}(\Phi)^2 = \alpha^2 2 f^2 A^2 + \beta^2 8 f^2 A^2.$$

We assume that synthesis of the slope RMS is in accordance with the Law of Squares. The square of the slope RMS through synthesis is shown as $(\sqrt{2\alpha^2 + 8\beta^2}\pi A f)^2$, which is equal to the result, by definition. So the synthesis of the wavefront, which is synthesized by two basal polynomials, satisfies the Law of Squares. The above conclusion can be extended to the Nth-order situation:

$$\text{slope RMS}^2 = \sum_i^N c_i^2\,\text{slope RMS}_i^2. \tag{5}$$

From Eq. (5), the overall slope RMS can be obtained by solving the slope RMS of each item when a standard orthogonal base, like standard sinusoidal polynomials, is used to represent the wave aberration. In practical engineering applications, the first few wave aberrations represented by the standard Zernike polynomial can be removed before completing the slope RMS calculation. For instance, in the evaluation of the GSSM surface, the data is normalized to the unit circle by using the Zernike polynomial to fit the defocusing and astigmatism terms. The rest of the data is processed as residual, considering the active adjustment ability of the primary mirror and the deformable mirror of the TMT.

The random process $\{X(t), t \in T\}$ by which the first and second moments exist is known as the second moment process.

Normally, without damage, the slope $\theta(x)$ of the wavefront aberration of the mirror surface measured by optical instruments cannot be unlimited. Thus, the first and second moments will exist.

We can obtain the correlation coefficient $R(\theta(x+r), \theta(x))$ of the second moment process by the use of the Cauchy–Schwartz Inequality:

$$R^2(\theta(x+r), \theta(x)) = \{E[\theta(x+r)\theta(x)]\}^2$$
$$\le E[\theta^2(x+r)]E[\theta^2(x)] < +\infty.$$

Therefore, the correlation coefficient $R(\theta(x+r), \theta(x))$ of the second moment process is always present, i.e., $R(\theta(x+r), \theta(x))$ always meet the requirements of the Fourier transform so that the power spectrum can be analyzed. Meanwhile, the second moment process in practical engineering mostly has fixed expectations and time invariance, so it can be considered as a wide smooth sequence. Then, the expectations can be estimated by the use of average time.

Power spectral analysis actually refers to PSD analysis, or spectral for short. For a wide smooth sequence with a zero mean, according to the Wiener's Theorem, the sequence power spectrum is the Fourier transform of the

autocorrelation sequence. In a practical optical system, the average of the wave aberrations of a mirror surface can be considered as the ideal surface. Because the GSSM of the TMT is a flat mirror with a large aperture, the random sequence generated by the mirror surface can be regarded as a wide smooth sequence with a zero mean:

$$S(\omega) = \sum_{-\infty}^{\infty} R(m) e^{-j\omega} = \sum_{-\infty}^{\infty} E[x(n)x^*(n+m)] e^{-j\omega}.$$

Note that ω is the circle frequency. The 2D case is considered below:

$$s(u,v) = \frac{1}{L'L} \times \left| \sum_{m=0}^{L'-1} \sum_{n=0}^{L-1} \omega(m,n) X(m+i'D', n+iD) e^{-j(mu+nv)} \right|^2.$$

Note that L', L is the length of the data in two different dimensions.

A 1D power spectrum has simple and intuitive features. This Letter introduces a method of 2D power spectrum collapse that uses wavefront information as much as possible while keeping the simple features of a 1D power spectrum.

A power spectrum collapse generally has two approaches: time-domain collapse or frequency-domain collapse. For time-domain collapse, the effect of the collapse relies strongly on the rotation symmetry of the wavefront. The numerical precision of the data has a large impact on the calculation of power spectrum. For frequency-domain collapse, due to the symmetry of the Fourier transform itself, the algorithm reduces the demands for rotation symmetry of the wavefront and improves the output quality of the power spectrum because of the average filtering effect.

The specific method of frequency-domain collapse is presented as follows: a 2D power spectrum is collapsed into one dimension by calculating the 2D power spectrum of the annular region and mean radius:

$$\bar{\rho}_i = \frac{1}{N_i} \sum_{N_{i-1}}^{N_i} \rho_l,$$

$$\mathrm{PSD}_{1\mathrm{D}} = \frac{1}{N} \sum_{N_{i-1}}^{N_i} \mathrm{PSD}_{2\mathrm{D}}(\rho_l),$$

where ρ_l is the radius of the power spectrum calculation.

Considering the form of the wavefront error given previously, the system wavefront error that corresponds to the unit bandwidth is shown as

$$\Delta\phi = \frac{A \sin(2\pi f x)}{\Delta f}, \tag{6}$$

where f is the spatial frequency.

The expression that is only associated with variables in the time domain can be obtained by integrating PSD into the frequency domain. Using the other definition of PSD, i.e., the energy corresponding to per unit frequency, which can be found by using Eq. (1), we can obtain

$$\mathrm{PSD} = \frac{A^2}{2\Delta f}, \tag{7}$$

which is the expression of the PSD at a single frequency or at the RMS value of the wavefront error corresponding to one frequency, in the case of multiple frequencies. The relationship between the slope RMS and the PSD is shown as

$$\begin{aligned} \text{Slope RMS}^2 &= \langle |\nabla\phi|^2 \rangle \\ &= 2\pi^2 \int \mathrm{PSD} \cdot f^2 \cdot \mathrm{d}f \\ &= 2\pi^2 \lim_{\Delta f \to 0} \frac{\int_f^{f+\Delta f} A f^2 \mathrm{d}f}{\Delta f} \\ &= 2\pi^2 f^2. \end{aligned} \tag{8}$$

Due to the fact that the result of Eq. (8) is the same as that of Eq. (2), the accuracy of Eq. (8) can be verified. Meanwhile, the slope RMS and PSD can be linked, using Eq. (8). Slope RMS takes advantage of the basal polynomial synthesis, can evaluate mid-frequency error, and represents the low frequency well. Particularly for active optics, its significance is more obvious. PSD is well able to represent the mid-frequency and can be related to atmospheric seeing conditions. So we can get a better quality evaluation when slope RMS and PSD are considered at the same time.

The system wavefront fitting can be mainly divided into three steps: removing the rigid displacement, solving the polynomial coefficients by using the normal equation, and processing residuals.

First, the piston and tip/tilt components of the wavefront are considered, as shown in

$$\begin{aligned} \Phi &= \sqrt{2} A \sin(2\pi f x), \\ \Phi' &= \sqrt{2} A \sin(2\pi f x) + \alpha x + \beta, \\ \Phi_{\mathrm{slope}} &= 2\sqrt{2}\pi f A \cos(2\pi f x), \\ \Phi'_{\mathrm{slope}} &= 2\sqrt{2}\pi f A \cos(2\pi f x) + \alpha. \end{aligned} \tag{9}$$

After a one-order difference, just the piston can be considered, i.e., wavefront information without a rigid displacement can be obtained by subtracting the average. Then, the solution of normal equation is studied. Only the defocusing and astigmatism of the Zernike polynomials in all directions (Z4, Z5, and Z6) are considered. Omitting the inner product notation, the normal equation fitting the original wavefront information is shown in

$$\begin{pmatrix} Z_4^2 & Z_4Z_5 & Z_4Z_6 \\ Z_4Z_5 & Z_5^2 & Z_5Z_6 \\ Z_4Z_6 & Z_5Z_6 & Z_6^2 \end{pmatrix}\begin{pmatrix} a_4 \\ a_5 \\ a_6 \end{pmatrix} = \begin{pmatrix} \phi Z_4 \\ \phi Z_5 \\ \phi Z_6 \end{pmatrix}. \tag{10}$$

By the derivation of Eq. (10), we can obtain

$$\begin{aligned} &d\begin{pmatrix} Z_4^2 & Z_4Z_5 & Z_4Z_6 \\ Z_4Z_5 & Z_5^2 & Z_5Z_6 \\ Z_4Z_6 & Z_5Z_6 & Z_6^2 \end{pmatrix}\begin{pmatrix} a_4 \\ a_5 \\ a_6 \end{pmatrix} = d\begin{pmatrix} \phi Z_4 \\ \phi Z_5 \\ \phi Z_6 \end{pmatrix} \\ &\begin{pmatrix} 2Z_4Z_4' & Z_4'Z_5 + Z_4Z_5' & Z_4'Z_6 + Z_4Z_6' \\ Z_4'Z_5 + Z_4Z_5' & 2Z_5Z_5' & Z_5'Z_6 + Z_5Z_6' \\ Z_4'Z_6 + Z_4Z' & Z_5'Z_6 + Z_5Z_6' & 2Z_6Z_6' \end{pmatrix}\begin{pmatrix} a_4 \\ a_5 \\ a_6 \end{pmatrix} \\ &= \begin{pmatrix} \phi' Z_4 + \phi Z_4' \\ \phi' Z_5 + \phi Z_5' \\ \phi' Z_6 + \phi Z_6' \end{pmatrix}. \end{aligned} \tag{11}$$

The measured data of the wavefront slope can be directly used to fit the lower-order system of the wavefront aberration. Then, the slope RMS, including the low frequency, can be obtained using the conclusion mentioned above.

Assuming that the wavefront of the sub-aperture is part of the Zernike polynomials of the overall wavefront, the Zernike coefficients of the whole wavefront can be obtained by fitting the sub-aperture. So the values corresponding to $\mathbf{\Phi}$ only consist of the measured positions of the sub-aperture.

The fitting residuals are required to process large aperture systems. We can deduce the requirements of the slope RMS by using the optical structure function and the optical transfer function from Eqs. (3) and (4). In the following, the analysis is done using the slope RMS combined with the specific requirements of the GSSM.

When gathering test data, the entire data (random sequence) of the mirror is in essence divided into several parts, between which the overlap is created. The approach of the window corresponds to the sub-aperture function (MASK) when using sub-aperture stitching. By combining sub-aperture stitching with a modified periodogram, the progressive unbiased estimate of the entire power spectrum can be obtained.

By using the previously obtained derivation, we can obtain the modified periodogram of each sub-aperture through the Welch method:

$$\begin{aligned} (\mathrm{PSD}_{\mathrm{sub}})_i = &\frac{1}{L'LU} \\ &\times \int_{-\pi}^{\pi}\int_{-\pi}^{\pi} S_{\mathrm{full}}(u-\theta', v-\theta)|M_i(\theta',\theta)|^2 \mathrm{d}\theta'\mathrm{d}\theta, \end{aligned}$$

where U is undetermined coefficient of correction. As the structure of each MASK is identical, the periodogram of each sub-aperture is equal:

$$\begin{aligned} E(\mathrm{PSD}_{\mathrm{sub}}) = &\frac{1}{L'LUKK'} \times KK' \\ &\times \int_{-\pi}^{\pi}\int_{-\pi}^{\pi} S_{\mathrm{full}}(u-\theta', v-\theta)|\,W(\theta',\theta)|^2 \mathrm{d}\theta'\mathrm{d}\theta, \\ U = &\frac{1}{L'L} \times \sum_{m=0}^{L'-1}\sum_{n=0}^{L-1}|\omega(m,n)|^2. \end{aligned} \tag{12}$$

By using Parseval's theorem and the fact that the energy of the time domain is equal to that of the frequency domain, we can obtain the following:

$$U = \frac{1}{L'L} \times \int_{-\pi}^{\pi}\int_{-\pi}^{\pi} |\,W(\theta',\theta)|^2 \mathrm{d}\theta'\mathrm{d}\theta.$$

By selecting the appropriate values of MASK,

$$\lim_{L',L\to\infty} \frac{1}{L'LU}|\,W(\theta',\theta)|^2 = \begin{cases} 1\,(\theta',\theta=0) \\ 0\,(\text{others}) \end{cases}.$$

Substituting the result into Eq. (12), we can obtain

$$\lim_{L',L\to\infty} E(\mathrm{PSD}_{\mathrm{sub}}) = \mathrm{PSD}_{\mathrm{full}}.$$

So the method in this Letter is a progressive unbiased estimate.

Consider

$$\mathrm{var}(\mathrm{PSD}_{\mathrm{sub}}) \approx \frac{1}{K'K}\mathrm{var}(\mathrm{PSD}_{\mathrm{full}}),$$

where K', K is the number of sub-apertures in two different dimensions.

When the number of sub-apertures approaches infinity, the method in this Letter provides a consistent estimate.

From the above analysis, the quality of the estimation can be significantly improved by adding the number of sampling points and sub-apertures. This matches well with the idea that we can evaluate optical mirrors with large apertures at a low cost and with a high resolution by using sub-aperture stitching. Furthermore, from Eq. (12), we can see that the algorithm's precision is directly related to the sub-aperture number and shape. Finally, the method in this Letter has further lowered the requirements of the instruments compared with traditional method.

Through the method mentioned above, we can obtain a low-frequency fluctuation by using the wavefront slope. Then, we can obtain the mid-frequency information by using the method of periodogram estimation. In the actual application, for a mirror that needs thorough analysis, we can analyze the power spectrum to get the mid-frequency component after removing lower-order aberrations by using the method shown above. For the system in which the supporting structure has no ability to regulate, the power spectrum is directly measured and analyzed to get the mid-frequency information.

The data of a mirror surface with a diameter of 1.23 m was obtained using a Zygo interferometer, as shown in Fig. 2. After segmentation by using MASK, the non-coherent sub-aperture stitching for the Φ1.23 m mirror based on the power spectrum was processed, as shown in Fig. 3. Nine sub-apertures and the square MASK were used, and the rate of overlap achieved 30%.

The mid-frequency not-to-pass (NTP) curve offered by the LLNL is added to Fig. 3. The cutoff frequency corresponding to the intersection between the surface power spectrum curve and the NTP curve is an important indicator of the system evaluation. The result obtained by the method of stitching is 10.5 m^{-1}, while the result by direct calculation is 11 m^{-1}. There is a difference of about 5%. In addition, the slope RMS of the mirror with a diameter of 1.23 m is 1.03 μrad. By using Eq. (2), we can obtain

$$f_0 = \frac{\text{slope RMS}}{\sqrt{2}\pi A} = 10.07\ \text{m}^{-1}.$$

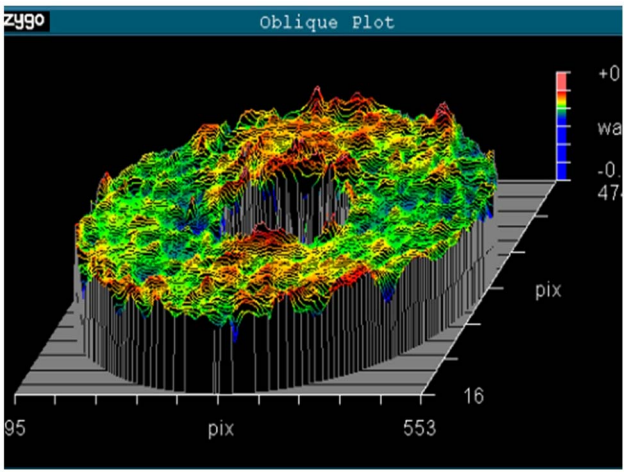

Fig. 2. The data of the mirror surface.

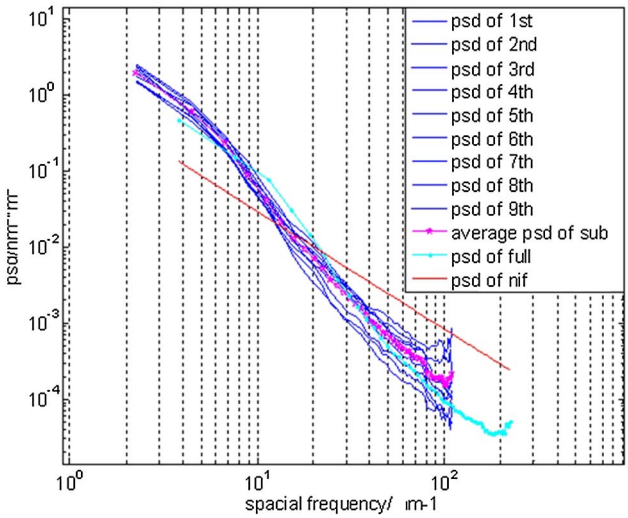

Fig. 3. Sketch of sub-aperture stitching of the Φ1.23 m mirror.

Through Eq. (3), the system structure function is shown in Fig. 4. We can see that the measured values are in good agreement with the empirical values for both the low and high frequencies. However, the gap between the measured values and the empirical values is large in the mid-frequency range. As the main specific features are concentrated in the mid-frequency range, if the range is well controlled, then the overall optical performance of system can be significantly improved. Combined with the power spectrum, we can obtain the overall evaluation. The combination of the cutoff frequency obtained by the power spectrum sub-aperture and the slope RMS is also considered, and can be an important indicator of performance.

The normalized mirror surface figure of GSSM is shown in Fig. 5 and the sketch of the sub-aperture stitching for GSSM by the method in this Letter is shown in Fig. 6. From the simulation result, we can see that the curve

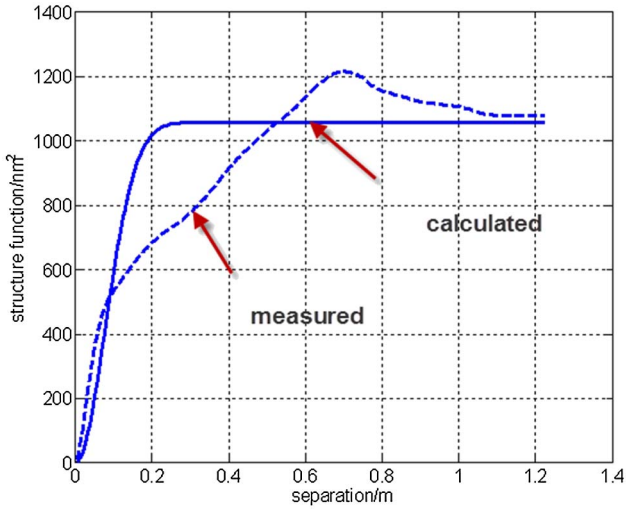

Fig. 4. Structural function of a Φ1.23 m reflecting mirror.

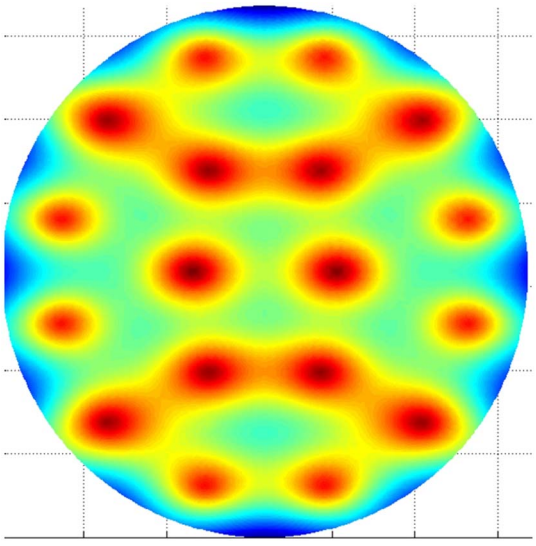

Fig. 5. Mirror surface of GSSM.

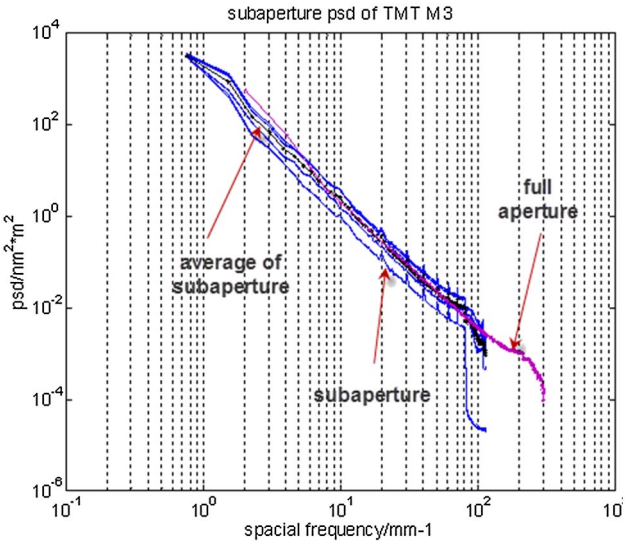

Fig. 6. Sketch of sub-aperture stitching for GSSM.

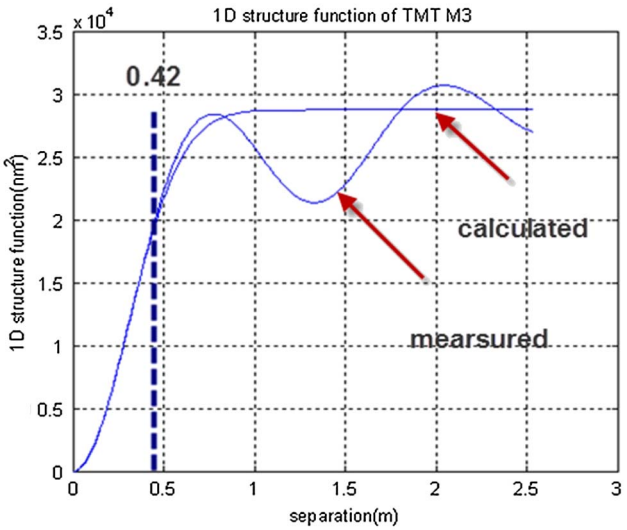

Fig. 7. Structural function of GSSM.

did not rise at a high frequency, but fell quickly at low frequency, indicating that the low-order fluctuations generated by gravity play major roles. In the actual test, we will coordinate with the TMT project about the selection of specific NTP curves to create social and economic benefits under the condition of the accuracy requirements.

For the GSSM surface, which has removed any defocusing and astigmatism, the slope RMS by is 0.98 μrad. By the use of Eq. (2), we can get $f_0 = \frac{\text{slope RMS}}{\sqrt{2}\pi A} = \frac{1}{4}$ m^{-1}, which is used as the cutoff frequency of the system.

Through Eq. (3), the system's structural function is shown in Fig. 7, which can be deduced by obtaining the spatial cutoff frequency using the slope RMS, in accordance with the structural functions in the medium and high bands, which are obtained by using the wavefront information. The result illustrates the accuracy of the method of solving the spatial cutoff frequency, and that the weaknesses of huge-volume data and the difficulty of the computations can be overcome. It also illustrates that this method is instructive in evaluating a large aperture mirror surface.

In conclusion, the usefulness of the slope RMS for evaluating mirror surface is analyzed, taking into consideration low-order wave aberrations and optical indicators. A new method of non-correlation sub-aperture stitching using PSD is also proposed. Its estimating quality is deduced and upheld by experiment. The TMT GSSM can not only be qualitatively analyzed by this method, but also quantitatively evaluated with NTP curve by a similar method in LLNL. The work has great value for the TMT project in the building, testing, and evaluation of a large aperture mirror surface.

This work was supported by the National Natural Science Foundation of China (NSFC) under Grant No. 11403022.

References

1. TMT Group, "Tertiary Mirrorsurface Figure Specification," TMT. OPT.SPE.12.001.DRF02 (2012).
2. TMT Group, "Design Requirements Document for Tertiary Mirror System (M3S)," TMT.OPT.DRD.07.006.REL29 (2012).
3. Y. Bi, J. Zhai, J. Wu, and Q. Hu, J. Opt. Tech. **35**, 10 (2009).
4. W. Zhang, J. Liu, F. Long, and Z. Wang, J. Opt. Tech. **31**, 675 (2005).
5. J. Chen, "*Principles of Astronomical Telescope Design*," (M. China Science & Technology Press, 2003).
6. X. Hu, W. Wang, Q. Hu, X. Lei, Q. Wei, Y. Liu, and J. Wang, Chin. Opt. Lett. **12**, 072901 (2014).
7. W. Dierking, Proc. IEEE **38**, 1451 (2000).
8. R. Zhelem, Proc. SPIE **8083**, 808310 (2011).
9. H. Shen, R. Zhu, Z. Gao, E. Y. B. PUN, W. H. Wong, and X. Zhu, Chin. Opt. Lett. **11**, 032201 (2013).